

# Constraining accretion efficiency in massive binary stars with LIGO–Virgo black holes

Yann Bouffanais,<sup>1,2\*</sup> Michela Mapelli,<sup>1,2,3</sup> Filippo Santoliquido,<sup>1,2</sup> Nicola Giacobbo,<sup>1,2,3</sup>  
Giuliano Iorio,<sup>1,2</sup> Guglielmo Costa<sup>1,2,3</sup>

<sup>1</sup>*Physics and Astronomy Department Galileo Galilei, University of Padova, Vicolo dell’Osservatorio 3, I–35122, Padova, Italy*

<sup>2</sup>*INFN-Padova, Via Marzolo 8, I–35131 Padova, Italy*

<sup>3</sup>*INAF-Osservatorio Astronomico di Padova, Vicolo dell’Osservatorio 5, I–35122, Padova, Italy*

Accepted XXX. Received YYY; in original form ZZZ

## ABSTRACT

The growing sample of LIGO–Virgo black holes (BHs) opens new perspectives for the study of massive binary evolution. Here, we study the impact of mass accretion efficiency on the properties of binary BH (BBH) mergers, by means of population synthesis simulations. We model mass accretion efficiency with the parameter  $f_{\text{MT}} \in [0.05, 1]$ , which represents the fraction of mass lost from the donor which is effectively accreted by the companion. Lower values of  $f_{\text{MT}}$  result in lower BBH merger rate densities and produce mass spectra skewed towards lower BH masses. Our hierarchical Bayesian analysis, applied to BBH mergers in the first and second observing run of LIGO–Virgo, yields almost zero support for values of  $f_{\text{MT}} \leq 0.3$ . This result holds for all the values of the common-envelope efficiency parameter we considered in this study ( $\alpha_{\text{CE}} = 1, 5$  and  $10$ ). The lower boundaries of the 95% credible intervals are equal to  $f_{\text{MT}} = 0.40, 0.45$  and  $0.48$  for  $\alpha_{\text{CE}} = 1, 5$  and  $10$ , respectively. This confirms that future gravitational-wave data can be used to put constraints on several uncertain binary evolution processes.

**Key words:** black hole physics – gravitational waves – methods: numerical – methods: statistical

## 1 INTRODUCTION

In 2015, the LIGO–Virgo collaboration (LVC) announced the first direct detection of gravitational waves (GWs) emitted by the merger of a binary black hole (BBH, Abbott et al. 2016b; Abbott et al. 2016c,a). In the first and second observing runs (hereafter, O1 and O2), nine additional BBHs and one binary neutron star (BNS) mergers were detected (Abbott et al. 2019a,b). In addition, Zackay et al. (2019), Udall et al. (2019), Venumadhav et al. (2020) and Nitz et al. (2020) claim several additional BBH candidates, based on an independent analysis of the O1 and O2 LVC data.

Four more events have already been reported from the third observing run (O3): the second BNS merger (GW190425, Abbott et al. 2020c), the first BBH with unequal mass components (GW190412, Abbott et al. 2020a), the most massive BBH merger ever observed (GW190521, Abbott et al. 2020b; Abbott et al. 2020e) and GW190814, whose secondary mass might be either the lightest black hole (BH) or the most massive neutron star (NS) ever observed (Abbott et al. 2020d). Furthermore, we expect that the total number of detections during O3 will significantly increase our current pool of detections<sup>1</sup>. This trend should further continue on with the improvement of current GW detectors and the upcoming third generation of GW detectors (Kalogera et al. 2019), Einstein Telescope (Punturo et al. 2010) and Cosmic Explorer (Reitze et al. 2019).

As a result of this increase in the number of detections, we are now capable of putting some constraints not only on single sources

parameters, but on the whole population of compact objects (Abbott et al. 2019b; Roulet & Zaldarriaga 2019). This gives us a unique opportunity to address some open questions on the astrophysics of these objects (Stevenson et al. 2017b; Mandel et al. 2019; Gerosa & Berti 2017; Fishbach et al. 2017; Fishbach et al. 2018; Fishbach & Holz 2020; Bouffanais et al. 2019; Callister et al. 2020).

The formation of BBHs from massive stars is usually studied by means of population synthesis codes, which trace the evolution of a massive binary system from its formation to the possible merger of its compact remnants (e.g., Tutukov & Yungelson 1973; Bethe & Brown 1998; Portegies Zwart & Yungelson 1998; Belczynski et al. 2002, 2008; Voss & Tauris 2003; Podsiadlowski et al. 2004; Belczynski et al. 2016; Eldridge & Stanway 2016; Stevenson et al. 2017a; Mapelli et al. 2017; Mapelli & Giacobbo 2018; Mapelli et al. 2019; Giacobbo & Mapelli 2018, 2020; Klencki et al. 2018; Kruckow et al. 2018; Vigna-Gómez et al. 2018; Eldridge et al. 2019; Spera et al. 2019; Tanikawa et al. 2020; Belczynski et al. 2020). Population-synthesis codes face the challenge of modelling several evolutionary stages which are still barely understood, such as common envelope (e.g., Webbink 1984; de Kool 1990; Ivanova et al. 2013; Fragos et al. 2019) and mass transfer. In particular, mass transfer via Roche lobe overflow (RLO) is a complex process and has a tremendous impact on the properties of massive binaries (e.g., Eggleton 2006). Different assumptions on the stability criteria for RLO mass transfer and on the onset of common envelope (e.g., Hjellming & Webbink 1987; Soberman et al. 1997; Murguía-Berthier et al. 2017; MacLeod & Loeb 2020) translate into dramatic differences on the statistics of BBHs (e.g., Dominik et al. 2012, 2013; de Mink & Mandel 2016; Mandel & de Mink 2016; Marchant et al. 2016).

\* E-mail: yann.bouffanais@gmail.com, bouffanais@pd.infn.it

<sup>1</sup> [gracedb.ligo.org](https://gracedb.ligo.org)

Another major uncertainty about RLO is represented by the fraction of mass lost from the donor star which is actually accreted by the companion (hereafter,  $f_{\text{MT}}$ ). Different codes either assume nearly conservative mass transfer (e.g., Hurley et al. 2002), or adopt a fiducial  $f_{\text{MT}} = 0.5$  (e.g., Belczynski et al. 2002, 2008) or prefer a highly non-conservative approach (e.g., Kruckow et al. 2018). Kruckow et al. (2018) test the behaviour of different values of  $f_{\text{MT}}$ , concluding that low values of mass accretion efficiency ( $f_{\text{MT}} \sim 0.25$ ) produce more realistic BNS masses.

Here, we investigate the impact of mass accretion efficiency on the mass spectrum and on the merger rate of BBHs by means of our binary population synthesis code MOBSE (Mapelli et al. 2017; Giacobbo et al. 2018). Exploiting Bayesian hierarchical analysis, we compare our simulated BBHs against LVC observations in O1 and O2 (Abbott et al. 2019a,b). We find that models with  $f_{\text{MT}} \leq 0.3$  struggle to match LVC observations, if we assume that isolated binary evolution is the only formation channel for BBHs.

## 2 ASTROPHYSICAL MODEL

### 2.1 Population synthesis

MOBSE<sup>2</sup> is a customized and upgraded version of BSE (Hurley et al. 2000, 2002), in which we included a new treatment for the evolution and the final fate of massive stars (Mapelli et al. 2017; Giacobbo et al. 2018; Giacobbo & Mapelli 2018).

Mass loss by stellar winds in massive hot ( $\geq 12500$  K) stars is described as  $\dot{M} \propto Z^\beta$ , where

$$\beta = \begin{cases} 0.85, & \text{if } \Gamma_e < 2/3 \\ 2.45 - 2.4\Gamma_e, & \text{if } 2/3 \leq \Gamma_e < 1 \\ 0.05, & \text{if } \Gamma_e \geq 1 \end{cases} \quad (1)$$

In the above equation,  $\Gamma_e$  is the electron-scattering Eddington ratio.

The outcome of core-collapse supernovae (SNe) is modelled following Fryer et al. (2012). In particular, we adopt the delayed model, in which the explosion is launched  $> 500$  ms after bounce. This model does not produce any mass gap between 2 and 5  $M_\odot$ . Stars with final carbon-oxygen mass  $m_{\text{CO}} \geq 11 M_\odot$  collapse to black hole (BH) directly. Following Timmes et al. (1996) and Zevin et al. (2020), we compute neutrino mass loss for both neutron stars (NSs) and BHs as

$$m_\nu = \min \left[ \frac{(\sqrt{1 + 0.3 m_{\text{bar}}} - 1)}{0.15}, 0.5 M_\odot \right], \quad (2)$$

where  $m_{\text{bar}}$  is the baryonic mass of the compact object. The resulting gravitational mass of the compact object is  $m_{\text{rem}} = m_{\text{bar}} - m_\nu$ . This leads to a maximum BH mass of  $\sim 65 - 70 M_\odot$  at low metallicity. As already discussed in Giacobbo & Mapelli (2018), even if we form BHs with mass up to  $\sim 65 M_\odot$ , only BHs with mass  $\leq 40 M_\odot$  merge within a Hubble time from isolated binary evolution, as an effect of mass transfer and common envelope in tight binary systems.

Prescriptions for pair instability SNe and pulsational pair instability SNe are also implemented, as described in Spera & Mapelli (2017) and Mapelli et al. (2020b). Our treatment for electron-capture SNe is described in Giacobbo & Mapelli (2019). Natal kicks are implemented as in Giacobbo & Mapelli (2020), assuming that  $v_{\text{kick}} \propto m_{\text{ej}} m_{\text{rem}}^{-1}$ , where  $m_{\text{ej}}$  is the mass of the ejecta. This model allows us to reproduce

**Table 1.** Summary of the models.

Model Name	$\alpha_{\text{CE}}$	$f_{\text{MT}}$
$\alpha 1$	1	0.05–1.0
$\alpha 5$	5	0.05–1.0
$\alpha 10$	10	0.05–1.0

Column 1: model name. Column 2: efficiency of common envelope ejection  $\alpha_{\text{CE}}$  of the CE. Column 3: mass accretion efficiency  $f_{\text{MT}}$ . We consider all values of  $f_{\text{MT}}$  from 0.05 to 1.0 by steps of 0.05.

both the proper motions of young pulsars in the Milky Way (Hobbs et al. 2005) and the merger rate inferred from LVC data (Abbott et al. 2020c).

In the original version of MOBSE, mass transfer via RLO is described as in Hurley et al. (2002). This yields a nearly conservative mass transfer if the accretor is a non-degenerate star. Here, we introduce an alternative model in which the mass accretion rate ( $\dot{m}_a$ ) is described as

$$\dot{m}_a = \begin{cases} f_{\text{MT}} |\dot{m}_d| & \text{if non-degenerate accretor} \\ \min(f_{\text{MT}} |\dot{m}_d|, \dot{m}_{\text{Edd}}) & \text{otherwise,} \end{cases} \quad (3)$$

where  $\dot{m}_d$  is the mass loss rate by the donor star,  $\dot{m}_{\text{Edd}}$  is the Eddington accretion rate and  $f_{\text{MT}} \in [0, 1]$  is the accretion efficiency. Here, we explore 20 values of  $f_{\text{MT}}$  ranging from 0.05 to 1 by steps of 0.05.

Other binary evolution processes such as wind mass transfer, tidal evolution, common envelope and GW energy loss are taken into account as described in Hurley et al. (2002). We explore three different values of the common envelope parameter  $\alpha_{\text{CE}} = 1, 5$  and 10 (Table 1). Small values of  $\alpha_{\text{CE}}$  mean that the binary must considerably shrink to eject the envelope, while large values of  $\alpha_{\text{CE}}$  translate into easy ejection. According to the original definition of  $\alpha_{\text{CE}}$  as the fraction of orbital energy which is efficiently transferred to the envelope (Webbink 1984), values larger than one should be deemed unphysical. However, several studies have shown that additional sources of energy play a role during common envelope, which are not accounted for in the original  $\alpha_{\text{CE}}$  model (e.g., Ivanova et al. 2013; Fragos et al. 2019). Moreover, values of  $\alpha_{\text{CE}} \geq 3$  seem to be in better agreement with the merger rate density of BNSs inferred from the LVC (Giacobbo & Mapelli 2020). Hence, in the following simulations, we adopt even values of  $\alpha_{\text{CE}}$  much larger than one.

We have considered 12 different stellar metallicities:  $Z = 0.0002, 0.0004, 0.0008, 0.0012, 0.0016, 0.002, 0.004, 0.006, 0.008, 0.012, 0.016, 0.02$ . For each run, we have simulated  $10^7$  binaries per each metallicity comprised between  $Z = 0.0002$  and 0.002, and  $2 \times 10^7$  binaries per each metallicity  $Z \geq 0.004$ , since higher metallicities are associated with lower BBH and BHNS merger efficiency (e.g. Giacobbo & Mapelli 2018; Kléncki et al. 2018). Thus, we have simulated  $1.8 \times 10^8$  binaries per each run (Table 1).

The mass of the primary is randomly drawn from a Kroupa initial mass function (Kroupa 2001) between 5 and 150  $M_\odot$ . We derive the mass ratio  $q = m_2/m_1$  as  $\mathcal{F}(q) \propto q^{-0.1}$  with  $q \in [0.1 - 1]$ , the orbital period  $P$  from  $\mathcal{F}(\Pi) \propto \Pi^{-0.55}$  with  $\Pi = \log_{10}(P/\text{day}) \in [0.15 - 5.5]$  and the eccentricity  $e$  from  $\mathcal{F}(e) \propto e^{-0.42}$  with  $0 \leq e \leq 0.9$  (Sana et al. 2012).

<sup>2</sup> <https://mobse-webpage.netlify.app/>

## 2.2 Merger rate density

To derive the merger rate density evolution of our models, we make use of the code `COSMORATE` (Santoliquido et al. 2020a,b):

$$\mathcal{R}(z) = \frac{d}{dt_{\text{lb}}(z)} \int_{z_{\text{max}}}^z \psi(z') \frac{dt_{\text{lb}}(z')}{dz'} dz' \times \int_{Z_{\text{min}}}^{Z_{\text{max}}} \eta(Z) \mathcal{F}(z', z, Z) dZ, \quad (4)$$

where  $t_{\text{lb}}(z)$  is the look-back time at redshift  $z$ ,  $Z_{\text{min}}$  and  $Z_{\text{max}}$  are the minimum and maximum metallicity,  $\psi(z')$  is the cosmic SFR at redshift  $z'$  from Madau & Fragos (2017),  $\mathcal{F}(z', z, Z)$  is the fraction of compact binaries that form at redshift  $z'$  from stars with metallicity  $Z$  and merge at redshift  $z$ , and  $\eta(Z)$  is the merger efficiency, namely the ratio between the total number  $N_{\text{TOT}}(Z)$  of compact binaries (formed from a coeval population) that merge within an Hubble time ( $t_{H_0} \lesssim 14$  Gyr) and the total initial mass  $M_*(Z)$  of the simulation with metallicity  $Z$ :

$$\eta(Z) = f_{\text{bin}} f_{\text{IMF}} \frac{N_{\text{TOT}}(Z)}{M_*(Z)}, \quad (5)$$

where  $f_{\text{bin}} = 0.5$  is the binary fraction, and  $f_{\text{IMF}} = 0.285$  is a correction factor that takes into account that only stars with mass  $m > 5 M_{\odot}$  are simulated. We refer to Santoliquido et al. (2020a) for more details on `COSMORATE`.

## 2.3 Analytical description of the model

For a given astrophysical model parametrised by  $\lambda$ , the population of merging BBHs is described as

$$\frac{dN}{d\theta}(\lambda) = N(\lambda) p_{\lambda}(\theta), \quad (6)$$

where  $\theta$  are the parameters of the merging BBHs,  $N(\lambda)$  is the total number of mergers predicted by the model and  $p_{\lambda}$  is the probability distribution associated with the parameters of the merging BBHs.

In practice, as we know that the GW detectors will not detect sources that are further away than a given horizon redshift  $z_h$ , we restrict ourselves to sources with redshift comprised between 0 and  $z_h$ , such that the number of detectable mergers in our model is,

$$N(\lambda) = \int_{z=0}^{z_h} \mathcal{R}(z) \frac{dV_c}{dz} \frac{T_{\text{obs}}}{1+z} dz, \quad (7)$$

where  $\mathcal{R}(z)$  is the merger rate density,  $dV_c/dz$  is the comoving volume element and  $T_{\text{obs}}$  is the observation time considered in the analysis. As our analysis is focused on sources detected by the LVC during the first two observing runs, we take a conservative value of  $z_h = 2$  for our horizon of BBHs.

To estimate our model distribution,  $p_{\lambda}(\theta)$ , we consider three parameters  $\theta = \{\mathcal{M}_c, q, z\}$ , where  $\mathcal{M}_c$  is the chirp mass and  $q$  the mass ratio. We do not consider the spins, because we assume that, at first order, spins are not affected by the efficiency of mass transfer. Hence, all the models we consider have the same spin distribution.

In practice, the distributions  $p_{\lambda}(\theta)$  were then estimated from a catalogue of  $N_{\text{tot}} = 50000$  sources representative of our model. Each entry of the catalogue gives the value of  $\theta = \{\mathcal{M}_c, q, z\}$  for the source, and we used kernel density estimation to obtain an estimation of  $p_{\lambda}(\theta)$ .

To construct our catalogues, we make use of the merger rate density inferred from `COSMORATE` to derive the expected distribution of sources between redshift 0 and  $z_h$ . Then, the code `COSMORATE` combines in good proportion the sources from the various catalogues

of metallicities simulated with `MOBSE`, such that we have the proper distribution of masses in the redshift intervals considered.

## 3 BAYESIAN INFERENCE

Bayesian analysis is widely used to analyse data from GW events. In particular, hierarchical Bayesian modeling has been the method of choice when doing model selection on population of compact binaries (Stevenson et al. 2015; Fishbach et al. 2017; Fishbach et al. 2018; Stevenson et al. 2017b; Gerosa & Berti 2017; Vitale et al. 2017; Zevin et al. 2017; Talbot & Thrane 2017, 2018; Mandel et al. 2019; Taylor & Gerosa 2018; Abbott et al. 2019b; Fishbach et al. 2017; Fishbach et al. 2018; Wysocki et al. 2018; Roulet & Zaldarriaga 2019; Kimball et al. 2020; Wong & Gerosa 2019; Vitale et al. 2019). In this section, we introduce the key concepts necessary to apply Bayesian analysis to a population of compact binaries.

### 3.1 Detector selection effects

As our detectors are not perfect, the observed population can significantly differ from the original population, resulting in selection effects on the observed distribution. One way to quantify the response of the interferometer to an incoming GW signal is to compute the quantity  $p_{\text{det}}(\theta)$ , which represents the probability that a source with parameter  $\theta$  is detected assuming one detector configuration (Finn & Chernoff 1993; Dominik et al. 2015). By making use of this quantity, we can filter our original catalogue following the method used in Bouffanais et al. (2019) and briefly summarised here.

For a given merging compact object signal, we can compute the value of its optimal signal to noise ratio (SNR),  $\rho_{\text{opt}}$ , corresponding to the case where the source is optimally oriented and located in the sky. All the uncertainties on the unknown position and orientation of the source can then be encoded in a parameter  $\omega$ , such that  $\rho = \omega \times \rho_{\text{opt}}$  where  $\rho$  is the actual SNR of the source and  $\omega \in [0, 1]$ . The detection probability can then be expressed as a function of  $\omega$  as,

$$p_{\text{det}}(\omega) = 1 - F_{\omega}(\rho_{\text{thr}}/\rho_{\text{opt}}), \quad (8)$$

where  $F_{\omega}$  is the cumulative function of  $\omega$  and  $\rho_{\text{thr}}$  is a SNR threshold for which the value  $\rho_{\text{thr}} = 8$  has been shown to be a good approximation of more complex analysis of detector network (Abadie et al. 2010; Abbott et al. 2016d; Wysocki et al. 2018). We use the python package `gwdet` (Gerosa 2019) to compute an approximation of  $F_{\omega}$  as a function of  $\omega$ .

The optimal SNR can be expressed as,

$$\rho_{\text{opt}} = 4 \int \frac{|\tilde{h}(f)|^2}{S_n(f)} df, \quad (9)$$

where  $\tilde{h}(f)$  is the waveform in the Fourier domain and  $S_n(f)$  is the one-sided noise power spectral density. In our case, we have used the IMRPhenomD waveform (Khan et al. 2016) computed via the package `PyCBC` (Dal Canton et al. 2014; Usman et al. 2016). For the detector sensitivity, we have considered the sensitivities of O1 and O2 separately. In practice, for each observing run we have computed the value of  $S_n(f)$  by averaging the values of the one-sided noise power spectral density of the LIGO Livingston detector on all GW detections observed during a given observing run. This implies that we are slightly overestimating our network of detectors as we are assuming a network of Livingston-like detectors, while in reality the sensitivity of Hanford and Virgo were lower for all observing runs.

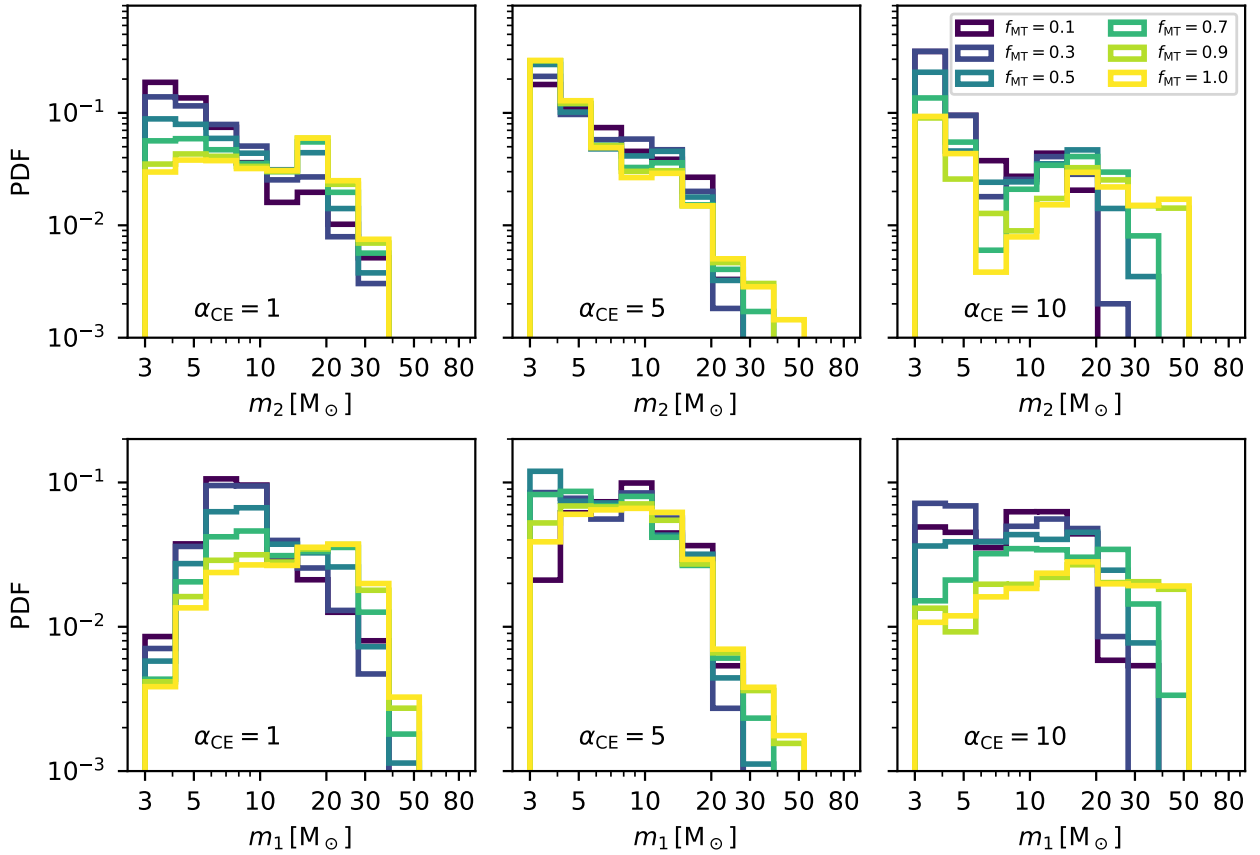


**Figure 1.** Upper panels ( $m_2$ ): masses of the secondary components of BBHs. Lower panels ( $m_1$ ): masses of the primary components of BBHs. From left to right:  $\alpha_{\text{CE}} = 1, 5$  and  $10$ . Different colors (from dark blue to yellow) refer to accretion efficiency  $f_{\text{MT}} = 0.1, 0.3, 0.5, 0.7, 0.9$  and  $1.0$ . These distributions are integrated over redshift.

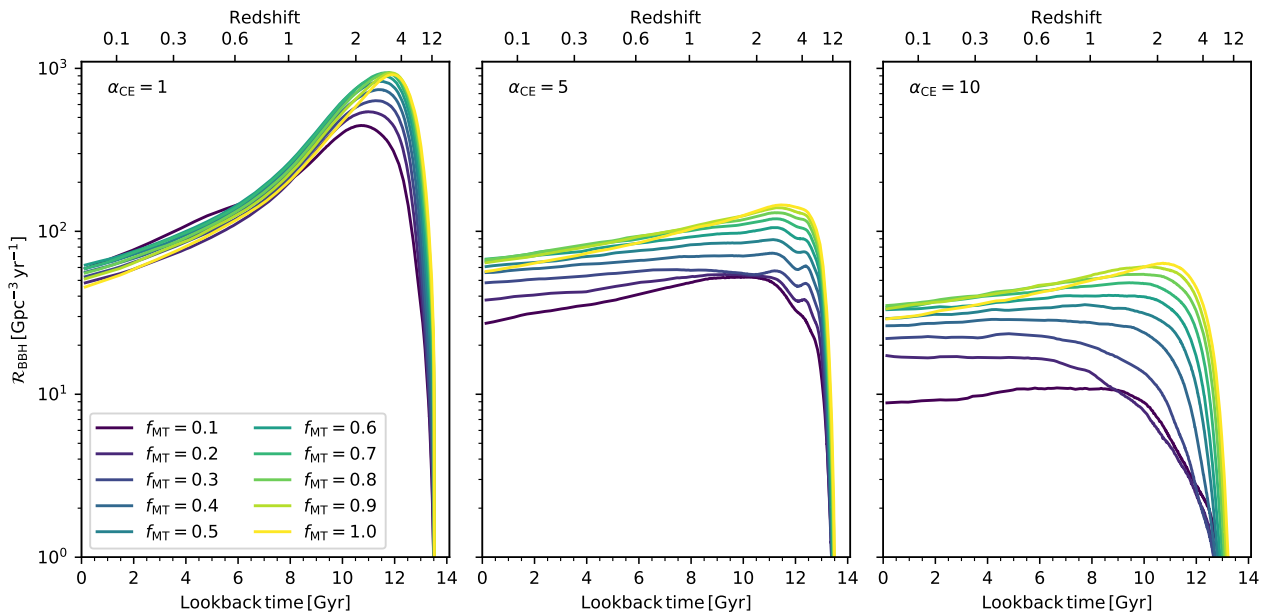


**Figure 2.** BBH merger rate density as a function of lookback time (lower  $x$ -axis) and redshift (upper  $x$ -axis). From left to right:  $\alpha_{\text{CE}} = 1, 5$  and  $10$ . Different colors (from dark blue to yellow) refer to accretion efficiency  $f_{\text{MT}} = 0.1, 0.2, 0.3, 0.4, 0.5, 0.6, 0.7, 0.8, 0.9$  and  $1.0$ .

### 3.2 Bayesian hierarchical modelling

As our Bayesian hierarchical analysis framework has already been presented in Bouffanais et al. (2019), here we only summarise the main equations. For a given set of  $N_{\text{obs}}$  GW detections  $\{h\}^k$ , the posterior distribution of our model parameter  $p(\lambda, N(\lambda) | \{h\}^k)$  is associated with a likelihood corresponding to an inhomogeneous Poisson process (Loredo 2004; Mandel et al. 2019)

$$\mathcal{L}(\{h\}^k | \lambda) \sim e^{-\mu(\lambda)} \prod_{k=1}^{N_{\text{obs}}} N(\lambda) \int \mathcal{L}^k(h^k | \theta) p_{\lambda}(\theta) d\theta, \quad (10)$$

where  $\mu(\lambda)$  is the predicted number of detections for the model and  $\mathcal{L}^k(h^k | \theta)$  is the likelihood of the  $k$ th detection. The predicted number of detections is expressed as

$$\mu(\lambda) = N(\lambda) \beta(\lambda), \quad (11)$$

where  $\beta(\lambda)$  is the detection efficiency of the model defined as

$$\beta(\lambda) = \int p_{\lambda}(\theta) p_{\text{det}}(\theta) d\theta, \quad (12)$$

where  $p_{\text{det}}(\theta)$  is the probability introduced in the previous section.

From a computational point of view, the detection efficiency in Eq (12) is approximated with a Monte Carlo approach as

$$\beta(\lambda) \approx \sum_i p_{\text{det}}(\theta_i), \quad (13)$$

where the sum is evaluated over sources with parameters  $\theta_i$ . These parameters are drawn from the distribution  $p_{\lambda}$  using a rejection sampling approach.

For the integral with the GW-event likelihood, we also use a Monte Carlo method to approximate the expression such that we have

$$\int \mathcal{L}^k(h^k | \theta) p_{\lambda}(\theta) d\theta \approx \sum_{i=1}^{N_s^k} \frac{p_{\lambda}(\theta_i^k)}{\pi^k(\theta_i^k)}, \quad (14)$$

where  $\theta_i^k$  is the  $i$ th sample of the  $N_s^k$  samples from the posterior distribution of the  $k$ th GW detection provided by the LVC and  $\pi^k$  is the prior distribution for the parameters of the  $k$ th detection that we approximate using kernel density estimation.

## 4 RESULTS

### 4.1 Mass Spectrum

Figure 1 shows the distribution of primary ( $m_1$ ) and secondary ( $m_2 \leq m_1$ ) components of BBH mergers for a selection of our models. The distributions are integrated over redshift, since we do not observe a significant trend with redshift. This figure clearly shows that both primary and secondary masses are affected by the accretion efficiency: larger values of  $f_{\text{MT}}$  leads to heavier BBH mergers. This trend seems to be stronger for  $\alpha_{\text{CE}} = 1, 10$ .

A small value of  $f_{\text{MT}}$  implies that only a small fraction of the mass lost from the donor star during mass transfer is accreted by the companion. Hence, the total mass of the final BBH system will be lower than in the case of  $f_{\text{MT}}$  close to one. For  $f_{\text{MT}} \sim 1$ , most primary BHs originate from the less massive progenitor, which accretes a significant fraction of mass from the companion. In contrast, if  $f_{\text{MT}} \sim 0.1$ , most primary BHs form from the most massive star in the original binary system.

### 4.2 Merger Rate Density

Figure 2 shows the merger rate density evolution of a selection of our models. The value of  $\alpha_{\text{CE}}$  has a strong impact on the merger rate, as already discussed in Santoliquido et al. (2020b): small values of  $\alpha_{\text{CE}}$  lead to a higher local merger rate density of BBHs and to a steeper slope with redshift. The Figure shows that the accretion efficiency also influences the merger rate: small values of  $f_{\text{MT}}$  lead to smaller BBH merger rate densities, especially for large values of  $\alpha_{\text{CE}}$ .

### 4.3 Posterior distribution

Figure 3 displays the posterior distribution of  $f_{\text{MT}}$ , as inferred from a MCMC chain produced via a Metropolis-Hastings algorithm run with the expression for the log-likelihood given in eq. (10) and assuming a uniform prior distribution for  $f_{\text{MT}}$ . The chain was run for  $10^7$  iterations, after which we discarded  $10^4$  as burn-in and trimmed the chains using the information from the autocorrelation length. In addition, as we simulated only 20 values of  $f_{\text{MT}}$ , we have used a linear interpolation of the logarithm of the likelihood between the two closest points to the targeted value of  $f_{\text{MT}}$ .

The most striking feature from the results in Figure 3 is that the posterior distributions have almost zero support for values of  $f_{\text{MT}} \leq 0.3$ . This result holds for all the values of  $\alpha_{\text{CE}}$ , with only a small peak around  $f_{\text{MT}} = 0.1$  for  $\alpha_{\text{CE}} = 1$ . From another perspective, the MCMC analysis reveals that the lower boundaries of the 95% credible intervals are respectively equal to  $f_{\text{MT}} = 0.40, 0.45$  and  $0.48$  for  $\alpha_{\text{CE}} = 1, 5$  and  $10$ , respectively. This means that with just the 10 BBH mergers from O1 and O2 (Abbott et al. 2019a), we are already able to put constraints on  $f_{\text{MT}}$ .

While it is difficult to disentangle all the elements playing a role in this analysis, it is possible to interpret this result by looking at the mass spectra presented in Fig. 1. In fact, smaller values of  $f_{\text{MT}}$  result in BH mass spectra skewed to lower masses, that struggle to represent the most massive BBHs already observed during O1 and O2 (namely, GW150914 and GW170729).

The second important feature in the posterior distribution of  $f_{\text{MT}}$  is the presence of multiple modes for  $f_{\text{MT}} > 0.3$ . This feature might result from the fact that we consider a discrete set of  $f_{\text{MT}}$  values, along with the linear fit taken to interpolate the values of the log-likelihood. We do not reject the possibility that the true posterior distribution of  $f_{\text{MT}}$  presents multiple modes, but our current analysis is not able to give enough confidence to answer this question. In the future, we plan to do an analysis with more values of  $f_{\text{MT}}$  to attenuate the effect of the grid. In addition, we would like to repeat the analysis with a GW catalogue that contains more observations (e.g., after the data release from the first part of O3), to put even more constraints on  $f_{\text{MT}}$ .

## 5 CONCLUSIONS

We studied the impact of mass accretion efficiency on the properties of BBH mergers, by means of population synthesis (run with the code `MOBSE`, Mapelli et al. 2017; Giacobbo et al. 2018) and Bayesian hierarchical analysis (Bouffanais et al. 2019). In particular, we assume that, during a RLO mass transfer, a non-degenerate star can accrete only a fraction  $f_{\text{MT}}$  of the mass lost by the donor. We consider  $f_{\text{MT}} \in [0.05, 1]$ . We repeat our calculations for three values of the common-envelope parameter  $\alpha_{\text{CE}} = 1, 5$  and  $10$ .

Models with low  $f_{\text{MT}}$  produce BBH mass functions skewed toward lower BH masses, because only a small fraction of the mass of the

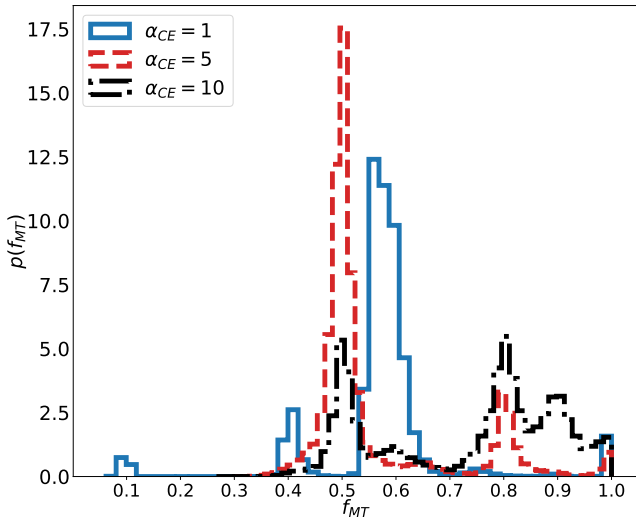


**Figure 3.** Posterior distribution of  $f_{\text{MT}}$ , as inferred from O1 and O2, for the models  $\alpha_{\text{CE}} = 1$  (blue solid line),  $\alpha_{\text{CE}} = 5$  (red dashed line) and  $\alpha_{\text{CE}} = 10$  (black dot-dashed line).

donor is accreted by the companion during the first Roche lobe mass transfer (Fig. 1).

Models with low  $f_{\text{MT}}$  also yield smaller BBH merger rate densities (Fig. 2). The impact of  $f_{\text{MT}}$  on the merger rate is stronger for larger values of  $\alpha_{\text{CE}}$ . If  $\alpha_{\text{CE}} = 10$ , the local BBH merger rate density spans from  $\sim 10 \text{ Gpc}^{-3} \text{ yr}^{-1}$  if  $f_{\text{MT}} = 0.05$  to  $\gtrsim 30 \text{ Gpc}^{-3} \text{ yr}^{-1}$  if  $f_{\text{MT}} \gtrsim 0.5$ .

We ran a hierarchical Bayesian analysis on our models against the LVC BBH mergers from O1 and O2 (Abbott et al. 2019a). The posterior distributions (Fig. 3) have almost zero support for values of  $f_{\text{MT}} \leq 0.3$ . This result holds for all the values of  $\alpha_{\text{CE}}$ . Our analysis reveals that the lower boundaries of the 95% credible intervals are equal to  $f_{\text{MT}} = 0.40, 0.45$  and  $0.48$  for  $\alpha_{\text{CE}} = 1, 5$  and  $10$ , respectively. Models with low  $f_{\text{MT}}$  are strongly disfavoured because they yield lower merger rate densities and steeper BH mass functions, which struggle to represent the most massive BBHs in O1 and O2.

Here, we made the strong assumption that isolated binary evolution is the only channel to form BBH mergers. Dynamical formation channels are expected to produce heavier BBH mergers than isolated binary evolution (e.g., Mapelli 2016; Zevin et al. 2017; McKernan et al. 2018; Di Carlo et al. 2019, 2020; Bouffanais et al. 2019; Rodriguez et al. 2019; Antonini et al. 2019; Mapelli et al. 2020a; Rizzuto et al. 2020; Fragione & Silk 2020; Arca Sedda et al. 2020; Banerjee et al. 2020). Hence, assuming that a fraction of the O1 and O2 BBHs have dynamical origin might possibly reconcile a low accretion efficiency ( $f_{\text{MT}} < 0.3$ ) with GW observations.

We expect that running our analysis on forthcoming O3 catalogues will lead to even stronger constraints on the efficiency of mass transfer. This result opens new perspectives on the possibility of understanding the process of mass transfer based on GW data.

## ACKNOWLEDGEMENT

We thank Erika Korb, Michele Guadagnin, Alessandro Lambertini, Alice Pagano and Michele Puppin for useful discussions on mass transfer. MM, YB, FS, NG, GI and GC acknowledge financial support

from the European Research Council for the ERC Consolidator grant DEMOBLACK, under contract no. 770017.

## REFERENCES

- Abadie J., et al., 2010, *Classical and Quantum Gravity*, **27**, 173001
- Abbott B. P., et al., 2016a, *Physical Review X*, **6**, 041015
- Abbott B. P., et al., 2016b, *Phys. Rev. Lett.*, **116**, 061102
- Abbott B. P., et al., 2016c, *ApJ*, **818**, L22
- Abbott B. P., et al., 2016d, *ApJ*, **833**, L1
- Abbott B. P., et al., 2019a, *Physical Review X*, **9**, 031040
- Abbott B. P., et al., 2019b, *ApJ*, **882**, L24
- Abbott B. P., et al., 2020a, arXiv e-prints, p. arXiv:2004.08342
- Abbott R., et al., 2020b, *Phys. Rev. Lett.*, **125**, 101102
- Abbott B. P., et al., 2020c, *ApJ*, **892**, L3
- Abbott R., et al., 2020d, *ApJ*, **896**, L44
- Abbott R., et al., 2020e, *ApJ*, **900**, L13
- Antonini F., Gieles M., Gualandris A., 2019, *MNRAS*, **486**, 5008
- Arca Sedda M., Mapelli M., Spera M., Benacquista M., Giacobbo N., 2020, *ApJ*, **894**, 133
- Banerjee S., Belczynski K., Fryer C. L., Berczik P., Hurley J. R., Spurzem R., Wang L., 2020, *A&A*, **639**, A41
- Belczynski K., Kalogera V., Bulik T., 2002, *ApJ*, **572**, 407
- Belczynski K., Kalogera V., Rasio F. A., Taam R. E., Zezas A., Bulik T., Maccarone T. J., Ivanova N., 2008, *ApJS*, **174**, 223
- Belczynski K., Holz D. E., Bulik T., O’Shaughnessy R., 2016, *Nature*, **534**, 512
- Belczynski K., et al., 2020, *A&A*, **636**, A104
- Bethe H. A., Brown G. E., 1998, *ApJ*, **506**, 780
- Bouffanais Y., Mapelli M., Gerosa D., Di Carlo U. N., Giacobbo N., Berti E., Baibhav V., 2019, *ApJ*, **886**, 25
- Callister T., Fishbach M., Holz D. E., Farr W. M., 2020, *ApJ*, **896**, L32
- Dal Canton T., et al., 2014, *Phys. Rev.*, **D90**, 082004
- Di Carlo U. N., Giacobbo N., Mapelli M., Pasquato M., Spera M., Wang L., Haardt F., 2019, *MNRAS*, **487**, 2947
- Di Carlo U. N., et al., 2020, arXiv e-prints, p. arXiv:2004.09525
- Dominik M., Belczynski K., Fryer C., Holz D. E., Berti E., Bulik T., Mandel I., O’Shaughnessy R., 2012, *ApJ*, **759**, 52
- Dominik M., Belczynski K., Fryer C., Holz D. E., Berti E., Bulik T., Mandel I., O’Shaughnessy R., 2013, *ApJ*, **779**, 72
- Dominik M., et al., 2015, *ApJ*, **806**, 263
- Eggleton P., 2006, *Evolutionary Processes in Binary and Multiple Stars*. Cambridge University Press
- Eldridge J. J., Stanway E. R., 2016, *MNRAS*, **462**, 3302
- Eldridge J. J., Stanway E. R., Tang P. N., 2019, *MNRAS*, **482**, 870
- Finn L. S., Chernoff D. F., 1993, *Phys. Rev. D*, **47**, 2198
- Fishbach M., Holz D. E., 2020, *ApJ*, **891**, L27
- Fishbach M., Holz D. E., Farr B., 2017, *ApJ*, **840**, L24
- Fishbach M., Holz D. E., Farr W. M., 2018, *ApJ*, **863**, L41
- Fragione G., Silk J., 2020, arXiv e-prints, p. arXiv:2006.01867
- Fragos T., Andrews J. J., Ramirez-Ruiz E., Meynet G., Kalogera V., Taam R. E., Zezas A., 2019, *ApJ*, **883**, L45
- Fryer C. L., Belczynski K., Wiktorowicz G., Dominik M., Kalogera V., Holz D. E., 2012, *ApJ*, **749**, 91
- Gerosa D., 2019, gwdet:Detectability of gravitational-wave signals from compact binary coalescences, doi:doi.org/10.5281/zenodo.889966.
- Gerosa D., Berti E., 2017, *Phys. Rev. D*, **95**, 124046
- Giacobbo N., Mapelli M., 2018, *MNRAS*, **480**, 2011
- Giacobbo N., Mapelli M., 2019, *MNRAS*, **482**, 2234
- Giacobbo N., Mapelli M., 2020, *ApJ*, **891**, 141
- Giacobbo N., Mapelli M., Spera M., 2018, *MNRAS*, **474**, 2959
- Hjellming M. S., Webbink R. F., 1987, *ApJ*, **318**, 794
- Hobbs G., Lorimer D. R., Lyne A. G., Kramer M., 2005, *MNRAS*, **360**, 974
- Hurley J. R., Pols O. R., Tout C. A., 2000, *MNRAS*, **315**, 543
- Hurley J. R., Tout C. A., Pols O. R., 2002, *MNRAS*, **329**, 897
- Ivanova N., et al., 2013, *A&ARv*, **21**, 59
- Kalogera V., et al., 2019, *BAAS*, **51**, 242

- Khan S., Husa S., Hannam M., Ohme F., Pürrer M., Jiménez Forteza X., Bohé A., 2016, *Phys. Rev. D*, 93, 044007
- Kimball C., Berry C., Kalogera V., 2020, *Research Notes of the AAS*, 4, 2
- Klencki J., Moe M., Gladysz W., Chruslinska M., Holz D. E., Belczynski K., 2018, *A&A*, 619, A77
- Kroupa P., 2001, *MNRAS*, 322, 231
- Kruckow M. U., Tauris T. M., Langer N., Kramer M., Izzard R. G., 2018, preprint, ([arXiv:1801.05433](https://arxiv.org/abs/1801.05433))
- Loredo T. J., 2004, *AIP Conf. Proc.*, 735, 195
- MacLeod M., Loeb A., 2020, *ApJ*, 893, 106
- Madau P., Fragos T., 2017, *ApJ*, 840, 39
- Mandel I., de Mink S. E., 2016, *MNRAS*, 458, 2634
- Mandel I., Farr W. M., Gair J. R., 2019, *MNRAS*, 486, 1086
- Mapelli M., 2016, *MNRAS*, 459, 3432
- Mapelli M., Giacobbo N., 2018, *MNRAS*, 479, 4391
- Mapelli M., Giacobbo N., Ripamonti E., Spera M., 2017, *MNRAS*, 472, 2422
- Mapelli M., Giacobbo N., Santoliquido F., Artale M. C., 2019, *MNRAS*, 487, 2
- Mapelli M., Santoliquido F., Bouffanais Y., Arca Sedda M., Giacobbo N., Artale M. C., Ballone A., 2020a, arXiv e-prints, [p. arXiv:2007.15022](https://arxiv.org/abs/2007.15022)
- Mapelli M., Spera M., Montanari E., Limongi M., Chieffi A., Giacobbo N., Bressan A., Bouffanais Y., 2020b, *ApJ*, 888, 76
- Marchant P., Langer N., Podsiadlowski P., Tauris T. M., Moriya T. J., 2016, *A&A*, 588, A50
- McKernan B., et al., 2018, *ApJ*, 866, 66
- Murguia-Berthier A., MacLeod M., Ramirez-Ruiz E., Antoni A., Macias P., 2017, *ApJ*, 845, 173
- Nitz A. H., Dent T., Davies G. S., Harry I., 2020, arXiv e-prints, [p. arXiv:2004.10015](https://arxiv.org/abs/2004.10015)
- Podsiadlowski P., Langer N., Poelarends A. J. T., Rappaport S., Heger A., Pfahl E., 2004, *ApJ*, 612, 1044
- Portegies Zwart S. F., Yungelson L. R., 1998, *A&A*, 332, 173
- Punturo M., et al., 2010, *Classical and Quantum Gravity*, 27, 194002
- Reitze D., et al., 2019, in BAAS. p. 35 ([arXiv:1907.04833](https://arxiv.org/abs/1907.04833))
- Rizzuto F. P., et al., 2020, arXiv e-prints, [p. arXiv:2008.09571](https://arxiv.org/abs/2008.09571)
- Rodríguez C. L., Zevin M., Amaro-Seoane P., Chatterjee S., Kremer K., Rasio F. A., Ye C. S., 2019, *Phys. Rev. D*, 100, 043027
- Roulet J., Zaldarriaga M., 2019, *MNRAS*, 484, 4216
- Sana H., et al., 2012, *Science*, 337, 444
- Santoliquido F., Mapelli M., Bouffanais Y., Giacobbo N., Di Carlo U. N., Rastello S., Artale M. C., Ballone A., 2020a, arXiv e-prints, [p. arXiv:2004.09533](https://arxiv.org/abs/2004.09533)
- Santoliquido F., Mapelli M., Giacobbo N., Bouffanais Y., Artale M. C., 2020b, arXiv e-prints, [p. arXiv:2009.03911](https://arxiv.org/abs/2009.03911)
- Soberman G. E., Phinney E. S., van den Heuvel E. P. J., 1997, *A&A*, 327, 620
- Spera M., Mapelli M., 2017, *MNRAS*, 470, 4739
- Spera M., Mapelli M., Giacobbo N., Trani A. A., Bressan A., Costa G., 2019, *MNRAS*, 485, 889
- Stevenson S., Ohme F., Fairhurst S., 2015, *ApJ*, 810, 58
- Stevenson S., Berry C. P. L., Mandel I., 2017a, preprint, ([arXiv:1703.06873](https://arxiv.org/abs/1703.06873))
- Stevenson S., Berry C. P. L., Mandel I., 2017b, *MNRAS*, 471, 2801
- Talbot C., Thrane E., 2017, *Phys. Rev. D*, 96, 023012
- Talbot C., Thrane E., 2018, *ApJ*, 856, 173
- Tanikawa A., Susa H., Yoshida T., Trani A. A., Kinugawa T., 2020, arXiv e-prints, [p. arXiv:2008.01890](https://arxiv.org/abs/2008.01890)
- Taylor S. R., Gerosa D., 2018, *Phys. Rev. D*, 98, 083017
- Timmes F. X., Woosley S. E., Weaver T. A., 1996, *ApJ*, 457, 834
- Tutukov A., Yungelson L., 1973, *Nauchnye Informatsii*, 27, 70
- Udall R., Jani K., Lange J., O’Shaughnessy R., Clark J., Cadonati L., Shoemaker D., Holley-Bockelmann K., 2019, arXiv e-prints, [p. arXiv:1912.10533](https://arxiv.org/abs/1912.10533)
- Usman S. A., et al., 2016, *Class. Quant. Grav.*, 33, 215004
- Venumadhav T., Zackay B., Roulet J., Dai L., Zaldarriaga M., 2020, *Phys. Rev. D*, 101, 083030
- Vigna-Gómez A., et al., 2018, *MNRAS*, 481, 4009
- Vitale S., Lynch R., Raymond V., Sturani R., Veitch J., Graff P., 2017, *Phys. Rev. D*, 95, 064053
- Vitale S., Farr W. M., Ng K. K. Y., Rodríguez C. L., 2019, *ApJ*, 886, L1
- Voss R., Tauris T. M., 2003, *MNRAS*, 342, 1169
- Webbink R. F., 1984, *ApJ*, 277, 355
- Wong K. W. K., Gerosa D., 2019, *Phys. Rev.*, D100, 083015
- Wysocki D., Gerosa D., O’Shaughnessy R., Belczynski K., Gladysz W., Berti E., Kesden M., Holz D. E., 2018, *Phys. Rev. D*, 97, 043014
- Zackay B., Venumadhav T., Dai L., Roulet J., Zaldarriaga M., 2019, *Phys. Rev. D*, 100, 023007
- Zevin M., Pankow C., Rodríguez C. L., Sampson L., Chase E., Kalogera V., Rasio F. A., 2017, *ApJ*, 846, 82
- Zevin M., Spera M., Berry C. P. L., Kalogera V., 2020, arXiv e-prints, [p. arXiv:2006.14573](https://arxiv.org/abs/2006.14573)
- de Kool M., 1990, *ApJ*, 358, 189
- de Mink S. E., Mandel I., 2016, *MNRAS*, 460, 3545

This paper has been typeset from a  $\text{\TeX}/\text{\LaTeX}$  file prepared by the author.